

Turbulent-boundary-layer development in an adverse pressure gradient after an interaction with a normal shock wave

By W. H. SCHOFIELD

Aeronautical Research Laboratories, Melbourne, Victoria, Australia

(Received 29 March 1984 and in revised form 20 November 1984)

An experimental study has been made of the development of a turbulent boundary layer in an adverse pressure gradient after an interaction with a normal shock wave that was strong enough to separate the boundary layer locally. The pressure gradient applied to the layer was additional to the pressure gradients induced by the shock wave. Measurements were taken for several hundreds of layer thicknesses downstream of the interaction. To separate the effects of shock wave and pressure gradient a second set of observations were made in a reference layer that developed in the same adverse pressure gradient without first interacting with a normal shock wave. It is shown that the adverse pressure gradient impressed on the flow downstream of the shock has a major effect on the structure of the interaction region and the growth of the layer through it. Consequently, existing results for interactions without a post-shock pressure gradient should not be used as a model for predicting practical flows, which typically have strong pressure gradients applied downstream of the shock wave. It is also shown that the shock wave produces a pronounced stabilizing effect on the downstream flow, which can be attributed to the streamwise vortices shed into the flow from the separated region formed by the shock wave. The implications of this result for nominally two-dimensional flow situations and to flows involving weak interactions without local separations are discussed.

1. Introduction

The problem of turbulent-boundary-layer development in an adverse pressure gradient that follows a normal shock wave strong enough to cause a local separation is relevant to several practical flows including air intakes on supersonic aircraft (Brown, Nawrocki & Paley 1968), transonic compressor stages (Leblanc & Goethals 1975), transonic diffusers (Sajben & Kroutil 1981) and transonic airfoils (Alstatt 1977). Given the practical importance of the flow and the difficulties in accurately predicting its development with current calculation methods (Vidal & Kooi 1976),† it is rather surprising that there have been so few experimental studies of the problem. The experimental studies involving both shock waves and post-shock pressure gradients that have been reported all have shortcomings. Padova, Falk & Wittliff (1980) and Vidal *et al.* (1973) both generated adverse pressure gradients downstream of a normal-shock-wave-boundary-layer interaction in blowdown Ludwig tubes but

† Moderate success in calculating boundary-layer development through an interaction with a shock wave has been demonstrated (Kline, Cantwell & Lilley 1982*b, c*) for simple cases that do not involve the coupled effects of shock wave and adverse pressure gradient on boundary-layer development.

their imposed post-shock pressure gradients were mild and their effects were observed over very limited distances downstream of the shock. More severe pressure gradients were used by Chen, Sajben & Krontil (1979) and Sajben & Krontil (1981), but, as their aim was to investigate oscillations in diffusers following shock-wave–boundary-layer interactions, they did not take measurements of boundary-layer development. This paper reports detailed measurements of boundary-layer development through an interaction with a normal shock wave and subsequently over an extended distance in a strong adverse pressure gradient.

Initially an attempt was made to devise an experiment relevant to all the practical flows listed above. Upon reflection it was considered that such an experiment was not really possible, as different boundary conditions for the different flows would give rise to significantly different three-dimensional components in the flow. The experimental layer studied here developed on the floor of a rectangular duct (see figure 1), and thus the flow was similar to that in a two-dimensional supersonic intake. Three-dimensional effects were important in the development of this flow, but comparisons with reference layers have enabled some general conclusions to be drawn from the present work.

The initial conditions of the layer before the shock wave are quite different in the practical flows listed above; they range from a favourable pressure gradient in transonic compressors and diffusers to adverse pressure gradients on some supersonic intakes. However, as all layers are impulsively separated by the shock wave and then subjected to vigorous mixing before reattachment, it is unlikely that details of the initial layer will be important to the downstream flow (Sajben & Krontil 1981), but they will of course be important in setting the scale for the interaction region (Hayakawa & Squire 1982).

In the absence of data on the combined effect of shock wave and adverse pressure gradient it is tempting (Inger 1975) to add the known effect of each agency in order to estimate the development of a boundary layer subjected to both. As turbulent boundary layers are highly nonlinear, a simple addition is, however, unlikely to give an accurate estimate. A different type of assumption that has been made (Livesey & Odukwè 1974) is that the development of a boundary layer over an extended distance in an adverse pressure gradient will be mainly determined by the pressure gradient, so that its final characteristics will be approximately the same whether the pressure gradient is preceded by a shock wave or not. This may also be inaccurate, as turbulent boundary layers have long memories of upstream events. To separate the effects of shock wave and pressure gradient in the present experiment, results were taken in a shock-free reference layer that developed in the same adverse pressure gradient as the main flow, but without a shock-wave interaction. Results by Seddon (1967) and others provide flat-plate data for layers that have interacted with a normal shock wave but in which the subsequent development was in zero pressure gradient. These three sets of results are used here to show how strong normal shock waves and adverse pressure gradients affect boundary-layer development individually and how they interact in combination.

2. Equipment and procedures

The experimental apparatus is shown diagrammatically in figure 1. An undried continuous air supply of 4.3 kg/s was preheated and maintained at a stagnation temperature of 403 ± 1 K before passing into a settling chamber 0.605 m in diameter containing six evenly spaced wire screens. The flow area was then reduced in a duct

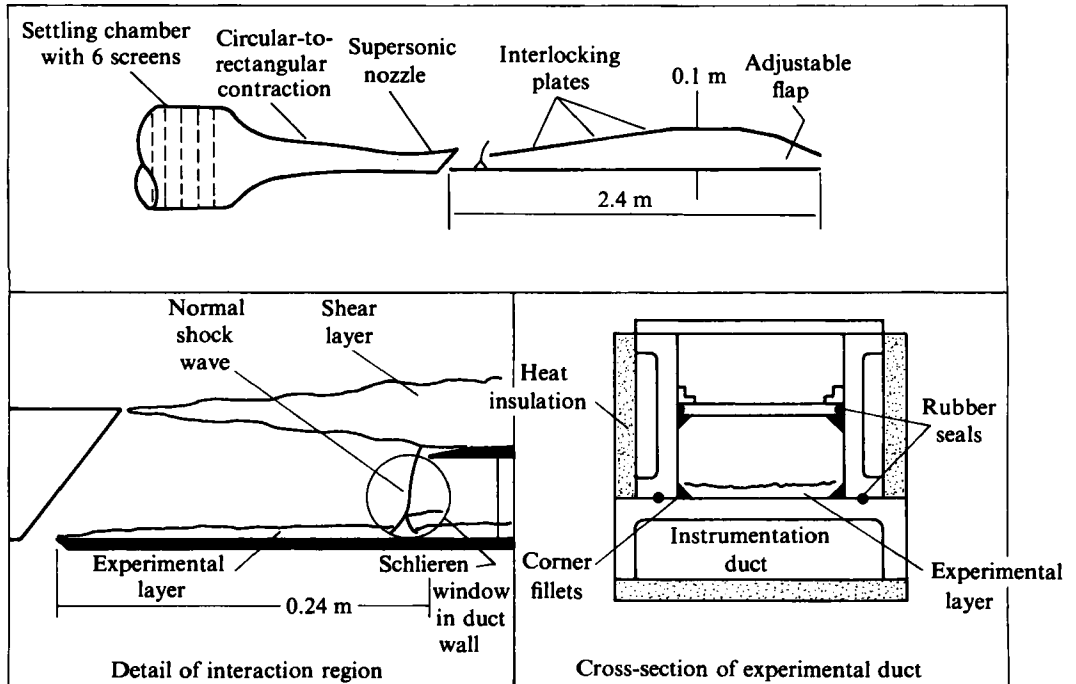


FIGURE 1. Diagram of experimental rig.

section that slowly changed from circular to rectangular before coming to a sonic throat with an overall area contraction ratio of 40 to 1. The flow was then accelerated to Mach 1.405, with an exit static temperature very close to ambient, giving the flow a unit Reynolds number of $3 \times 10^7 \text{ m}^{-1}$. The exit size of the nozzle was $99 \text{ mm} \times 82 \text{ mm}$ high, but the entrance to the experimental duct was smaller in both dimensions so that some of the nozzle flow was spilt around the sides of the duct. Thus none of the nozzle boundary layers entered the duct, and the heat loss from the forward part of the duct (which could not be lagged) was minimized by having similar flow on both sides of its walls. Downstream of the nozzle exit the duct walls were well insulated to produce nearly adiabatic flow within the duct. The duct was constructed from aluminium castings fitted with hardened-steel leading edges.

The experimental layer thus started at a leading edge in unsheread flow had a natural transition to a turbulent layer while developing in a zero pressure gradient. Surface-oil-flow studies suggested that transition was complete at 20 mm from the leading edge and occurred uniformly across the floor of the duct. The distance from the leading edge to the shock wave was 0.24 m, which allowed a layer of total thickness approximately 3.3 mm to be generated before the interaction. This gave a duct-width to layer-thickness ratio of 26:1, which is the same as in the experiment of Seddon (1967) that provides one of the main reference layers used in this work. Another comparison layer by Kooi (1975) had a relatively wider duct (ratio 40:1).

The height of the duct entrance was 47 mm, but increased with distance downstream so that the post-shock flow was subjected to an adverse pressure gradient. The roof was made of interlocking plates that were adjusted to generate a pressure gradient that was strong but did not re-separate the layer downstream of the shock wave. The sidewalls of the duct were set on slight angles to the centreline of the floor to

compensate for the (calculated) growth in the sidewall boundary-layer displacement thickness. Although the duct width thus increased (from 85 to 100 mm), the total layer thickness increased more rapidly, and at the end of the measurement region the layer-thickness to duct-width ratio was approximately 1:4.

Just downstream of the shock wave, fillets were attached to all four inner corners of the duct (see figure 1) to reduce secondary flows. The thickness of these fillets increased (from zero) with distance down the duct. Surface flow visualization indicated that the duct flow (away from the shock wave) was two-dimensional, that there was no leakage from the duct and that the boundary layers did not reseparate after the shock wave.

The floor of the duct was pressure-tapped with 46 small holes spaced along the plate in two rows 6.4 mm either side of the centreline. The floor plate also contained instrumentation holes on the duct centreline through which a variety of probes could be introduced into the duct. When not used for holding a probe the holes were filled with plugs containing static-pressure taps and thermocouples set flush with the flow surface in copper beads. The total head probes had flattened, square openings measuring (typically) 1 mm \times 0.12 mm. The temperature probe, a standard ventilated stagnation probe, had a square opening 5 mm \times 0.38 mm high. The static probe was 2 mm in diameter, with an elliptical nose and four equispaced circumferential holes. The quality of the probe tips and the accurate sizes of their openings were determined by generating images of them with a magnification of 100. All thermocouples were referred to a junction maintained at 0 °C with an accuracy better than 0.1 °C. Thermocouple voltages were measured directly with a calibrated digital voltmeter, which had a resolution of 1 μ V. Every temperature probe and wall thermocouple was extensively calibrated in a slowly heated stirred bath against substandard calibrated thermometers that could be read to within 0.02 °C. Check recalibrations were performed throughout the experiment. All temperature readings in the duct were normalized with the settling-chamber temperature, which was recorded with each experimental temperature reading. In reducing temperature-probe measurements a recovery factor (that was a weak function of Mach number) was used and typically had a value near 0.995. Except for the miniature probes used in the reversed-flow region, the openings of all probes were nominally 75 mm from the probe stem. Accurate measurements of this length were made so that, for traverses in regions of rapid longitudinal variation of velocity, corrections due to small mismatches in this length between different types of probes could be made. The probes were attached to the duct with a traverse mechanism that could generate steps as small as 0.008 mm. Probe position was determined with a distance transducer that had been extensively calibrated in an oven for a range of temperatures that corresponded with wall temperatures along the experimental duct. The wall contact position of a probe was found with a technique that was reliable within 0.01 mm. Probes and wall pressure tappings were connected with short lengths of tubing to strain-gauge pressure transducers. These transducers were periodically calibrated against a dead-weight tester and showed a maximum variation of less than 1% in sensitivity between calibrations. Typical variations were, however, considerably less than 1%. The zero-pressure reading of each transducer was recorded at the end of each run, as the zero-pressure constants were found to be weak functions of temperature. One absolute transducer was used to measure all static pressures with the aid of a scanivalve, while another difference transducer compared the local wall static to the probe pressure. In this way, dynamic-head or static-pressure deviation from wall static was measured directly. To eliminate the (small) effects of variation in

stagnation pressure, all pressure readings in the duct were normalized with the settling-chamber pressure, which was recorded with each experimental pressure.

An uncertainty analysis using the method of Kline & McClintock (1953) gave the uncertainties listed in table 1. The calculations involved errors that could be quite accurately assessed, except for the backflow. Here the contribution to the uncertainty due to the effect of an upstream probe stem was arbitrarily assigned at $\pm 5\%$ as no reliable experimental data on the effect could be found by the author. Another area not accurately assessed concerns quantities involving static-pressure measurements in flow with Mach numbers 0.9–1.1.†

Continuous viewing of the normal shock wave was afforded through the duct windows (shown in figure 1) with a schlieren system. The system had the ability to take photographs of the instantaneous schlieren pattern by illuminating it with a short-duration spark.

For each run the settling-chamber pressure was matched to the ambient pressure in order to give a correctly expanded jet at Mach 1.405 from the nozzle. This flow was uniform to within ± 0.01 of a Mach number across the jet at all cross-sections along the jet up to the shock-wave position (see Schofield 1975). The control over the settling-chamber pressure and temperature was sufficiently fine to hold the Mach number constant within ± 0.002 during every run. After the flow was established, the rear flap on the duct was adjusted until a normal shock wave appeared just upstream of the leading edge of the duct roof. Flow conditions were then allowed to stabilize for thirty minutes before the pressure distribution along the duct was recorded. Another such pressure distribution was recorded after the profile was taken. This procedure ensured that the pressure distribution was constant throughout the test and also that it did not vary across tests. At each point in a profile recording, values of wall static pressure and wall temperature were measured and used as instantaneous values in the data reduction, although the variation with time of these quantities was always small. No corrections for displacement or turbulence were made to the probe readings. Mean-velocity profiles were obtained by a suitable combination of total pressure and static pressure with temperature profiles. For stations at which a temperature profile was not measured the simple linear Crocco relation was used.

When the measurements in this main layer had been taken, an identical set of measurements were made in a shock-free reference layer. To produce this flow the settling-chamber pressure was reduced so that the Mach number at the nozzle exit and duct entrance was 0.61. This Mach number is somewhat lower than the post-shock Mach number (0.74) behind a normal shock wave at Mach 1.4, but was the highest that could be generated without causing some supersonic flow and waves in the nozzle. This small difference in Mach number is unimportant when comparing the development of the two boundary layers. For this new flow, conditions were again allowed to stabilize for thirty minutes before the same data-acquisition procedure as before was followed.

3. Results

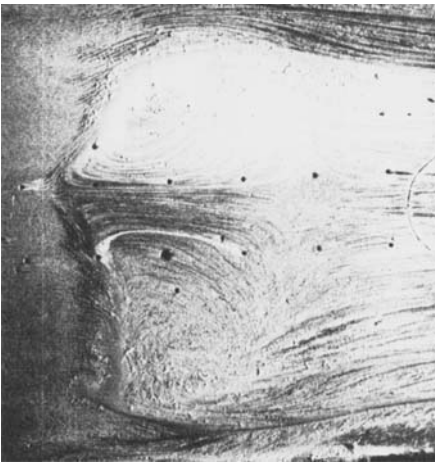
Two methods were used to estimate the stability of the shock wave. First, a large number of spark schlieren photographs taken at random times were compared. Secondly, records of pressure fluctuations at a single pressure tapping‡ near the centre

† This, however, involves only the static pressure in the outer part of one profile, which is not important to the analysis or description of the interaction flow (see the discussion of figure 6).

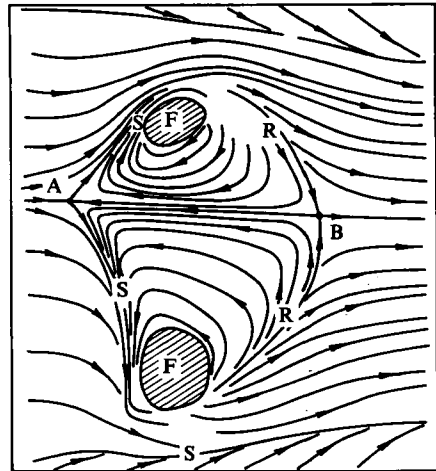
‡ Connected to a high-response transducer by a short length of tubing.



(a)



(b)



(c)

FIGURE 2. Surface-oil-flow pattern in the interaction region: (a) downstream view; (b) plan view; (c) schematic interpretation of (b). A, separation saddle point; B, reattachment saddle point; F, focus; S, separation line; R, reattachment line.

of the shock pressure rise were analysed and related to the shock position via the curve of mean-pressure rise versus distance along the duct. Both methods suggest a maximum shock excursion from the mean of order ± 1 mm, with an r.m.s. value about half this amount.

The schlieren pictures show the normal shock wave bifurcating into forward- and rearward-facing oblique shock waves at a point about seven (undisturbed) layer thicknesses above the plate. Similar pictures are shown in Seddon (1967) for the flat-plate interaction. In both flows a separation bubble under the shock wave is responsible for the bifurcation. Surface flow patterns (figures 2a, b) show that the flow is highly three-dimensional. Features of the separated region have been labelled in figure 2(c). The layer separates along lines (separatrices) emanating from a separation saddle point and reattaching along separatrices running into a reattachment saddle. On each side of the separated region the flow winds up into two (counter-rotating)

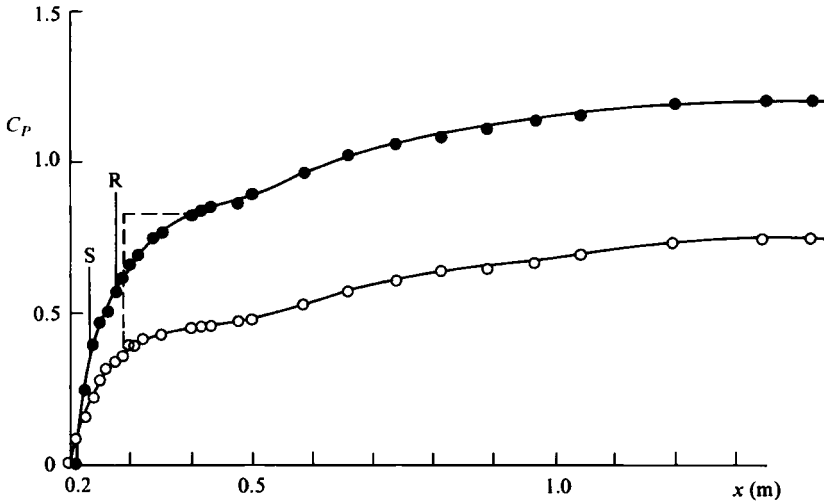


FIGURE 3. Wall-pressure distributions: ●, shock-interaction layer; ○, shock-free reference layer; ---, inviscid pressure rise without a post-shock pressure gradient; S, position of boundary-layer separation saddle; R, position of boundary-layer reattachment saddle.

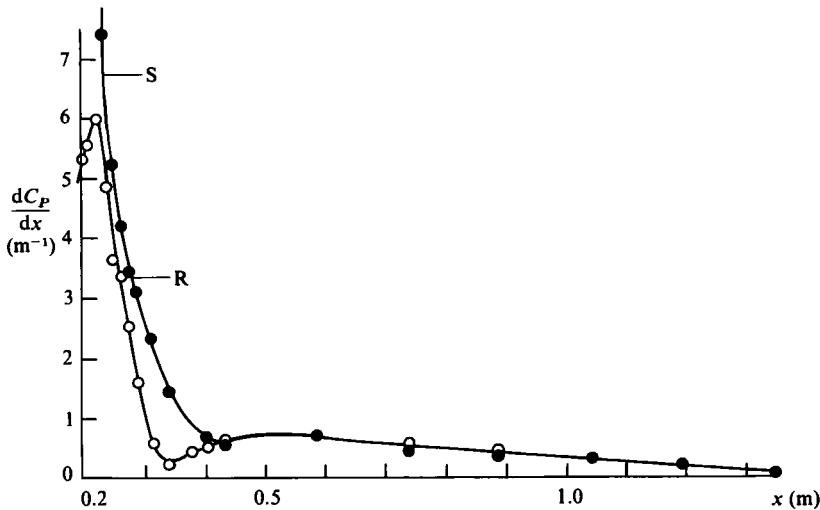


FIGURE 4. Pressure gradients. Symbols and notation as for figure 3. At those stations where only one point is shown the values for both layers are identical.

foci.† A rather similar pattern and interpretation was given by Green (1969) for an interaction of a turbulent boundary layer with a strong oblique shock wave in a square duct. Hunt *et al.* (1977) have made a detailed study of such separated regions in which they concluded that the separated flow was not enclosed by a single stream surface and that the foci on the wall were origins for two counter-rotating vortices shed downstream. The two conclusions were, of course, related, as there must be a mass influx into the separated region to supply the mass efflux of the shed vortices.

† Definitions of a focus and other critical points in surface flow patterns are given in Perry & Fairlie (1974).

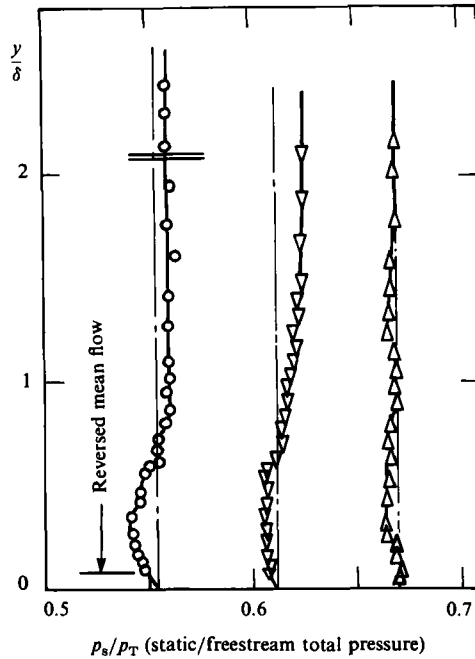


FIGURE 5. Static-pressure profiles: ○, 0.2762 m (19 layer thicknesses from start of interaction); ▽, 0.3143 m; △, 0.4031 m; reattachment at 0.280 m; δ is the total layer thickness; —, approximate position of the shear layer shed from the bifurcation of the shock wave; ---- wall static pressure.

The wall-pressure distributions† for the shock wave and shock-free reference flow are shown in figure 3, and the pressure gradients derived from these data are shown in figure 4. Downstream of the shock-wave region the pressure gradients for the two flows are closely similar. Therefore outside the interaction region the two layers have the same pressure histories.

The separated region under the shock wave will have non-negligible static-pressure gradients in the vertical and lateral directions as well as in the longitudinal direction. Limited lateral pressure measurements and detailed vertical pressure profiles, such as those shown in figure 5, suggest that these variations are moderate. The static-pressure results from experiments on flat plates and supersonic corners (Seddon 1967; Kooi 1975; Settles, Vas & Bogdonoff 1976) also show moderate variations. However, the magnitude and sign of the static-pressure deviation from wall static differs markedly between these experiments. It seems likely that the interaction between the separated flow, the static-pressure probes and the flow geometry may be significant and different between experiments (see Bradshaw *et al.*, p. 23 in Kline *et al.* 1982*a*). In the present experiment, for stations at which static-pressure profiles were not measured, the wall pressure was assumed constant throughout the profile. This of course results in a higher uncertainty for these profiles (see table 1).

3.1. Mean-velocity field

The undisturbed boundary layer before the interaction was a zero-pressure-gradient equilibrium turbulent boundary layer. It was accurately fitted by standard wall-wake

† Expressed in terms of $C_p = P/P_{at} - 1$, where P_{at} is atmospheric pressure.

| | Mach number (M) | Mean velocity (u) | Stream function (ψ) | Normalized temperature (\bar{T}) |
|---------------------------------------|---------------------------|-----------------------------|----------------------------------|--|
| (a) Measured p_s , T | | | | |
| near interaction | $\pm 1.2\%$ | $\pm 1.2\%$ | $\pm 1.5\%$ | $\pm 4.2\%$ |
| downstream of interaction | $\pm 1.0\%$ | $\pm 1.0\%$ | $\pm 1.3\%$ | $\pm 2.5\%$ |
| (b) Measured T , wall p_s | | | | |
| near interaction | $\pm 2.7\%$ | $\pm 2.7\%$ | $\pm 4.0\%$ | $\pm 4.2\%$ |
| downstream of interaction | $\pm 1.5\%$ | $\pm 1.5\%$ | $\pm 1.7\%$ | $\pm 2.5\%$ |
| (c) Crocco T , wall p_s | | | | |
| near interaction | $\pm 2.7\%$ | $\pm 2.8\%$ | $\pm 4.2\%$ | — |
| downstream of interaction | $\pm 1.5\%$ | $\pm 1.5\%$ | $\pm 1.8\%$ | — |
| backflow region | $\pm 6.5\%$ | $\pm 6.8\%$ | $\pm 7.4\%$ | — |
| Skin-friction coefficient = $\pm 5\%$ | | | | |
| Entrainment rate = $\pm 15\%$ | | | | |

TABLE 1. Estimated uncertainties of derived quantities. Wall p_s means profiles in which the wall static pressure is assumed constant throughout the profile. Crocco T means profiles in which the local static temperature is estimated using the Crocco linear relation.

similarity with a wake strength factor of 0.76 (see Schofield 1983). The boundary-layer profiles in the interaction region are shown in figure 6, where the (centreline) streamline pattern† constructed from the profiles is presented. The data in this figure show good internal consistency, in that streamline flow angles agree with the flow deflections of the shock system, and values of the stream function given by the different profiles form a consistent streamline pattern. In cases of minor disagreement in ψ -values between adjacent profiles, more weight has been given to data derived from profiles with low uncertainty.‡ The edge of the reversed flow could be quite accurately placed in figure 6 from the velocity profiles obtained from forward-facing probes. However, the high inaccuracy of the reversed-flow measurements means that values of the stream function immediately above the reversed flow, and hence the size of the recirculating flow, has a high uncertainty. This uncertainty in ψ reduces with distance from the wall as the integration for ψ incorporates more accurate data. The shape and size of the recirculating bubble must, however, be largely correct, as the angles of the computed streamlines above the bubble accord fairly accurately with the adjacent flow-deflection angles produced by the shock system. Another minor factor that affects the accuracy of this diagram is that the line of symmetry of the separated flow does not coincide with the duct centreline (see figure 2), and thus cross-flows on the duct centreline may not be negligible. The streamline pattern of figure 6 is compared with the corresponding patterns presented by East (1976) and Seddon (1967) for flat-plate flow in figure 7. The comparison shows that the addition of a strong post-shock adverse pressure gradient after the shock wave substantially modifies the flow structure in the interaction region by delaying reattachment of the layer and thus creating a larger separated-flow region. The rapid increase in the displacement thickness of the layer after it separates causes Mach-line compression that progressively bends and steepens the leading oblique shock wave, producing a

† In terms of ψ the compressible stream function.

‡ In figure 6, profiles with higher reliability were at $x = 0.276$ m, 0.314 m (static pressure and temperature profiles measured) and $x = 0.225$ m, 0.250 m (temperature profiles measured).

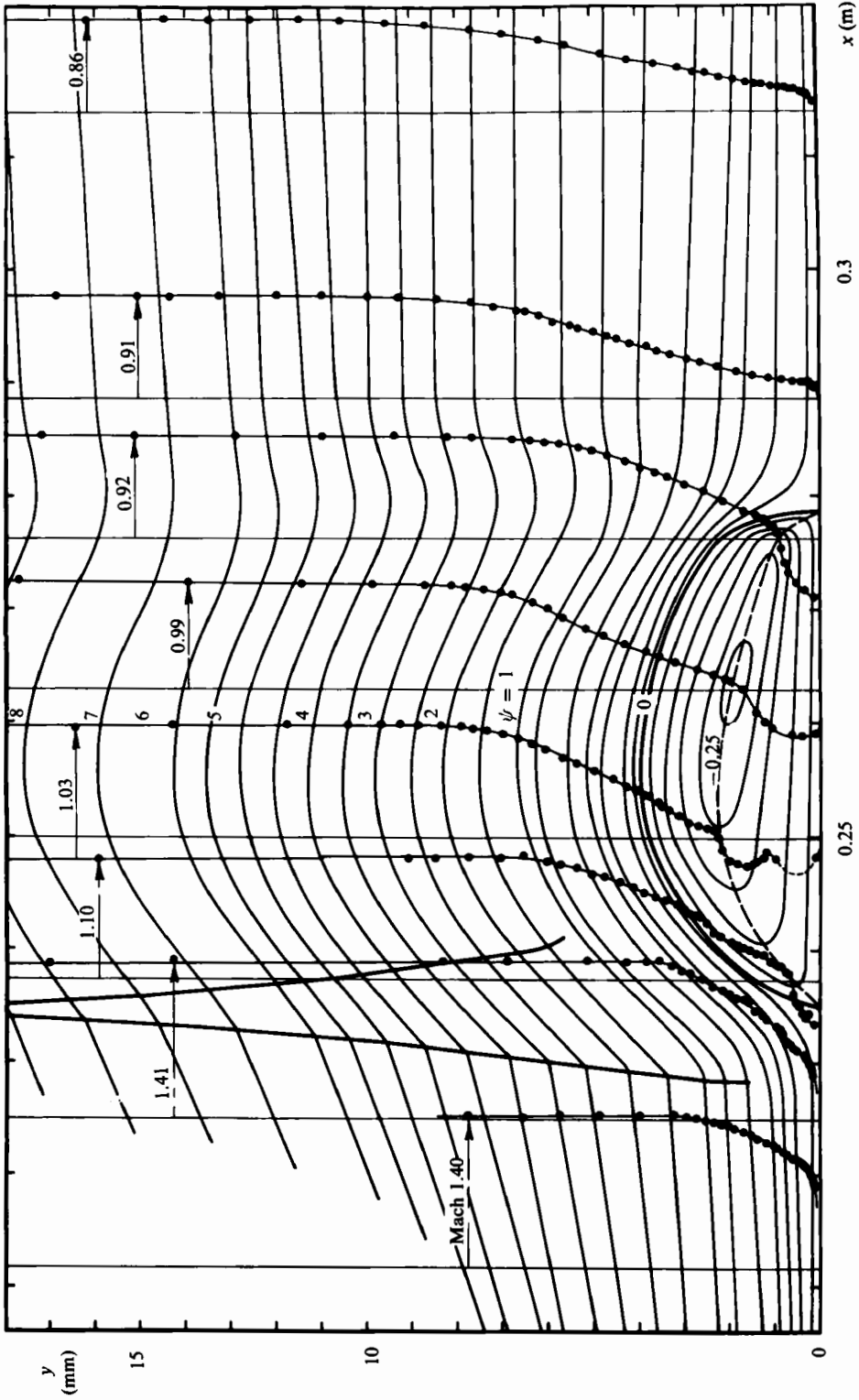


FIGURE 6. Streamlines from mean centreline profiles in the vicinity of the interaction. Note that the vertical scale is four times the horizontal scale. Units for ψ are $\text{kg m}^{-1} \text{s}^{-1}$.

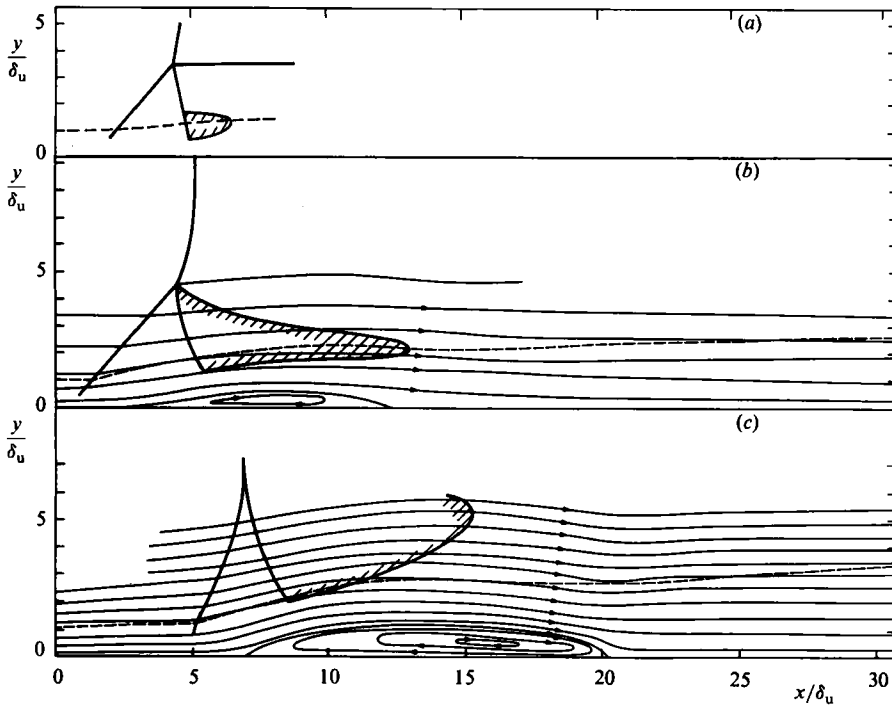




FIGURE 7. Streamlines from mean profiles for flows with and without a post-shock pressure gradient: (a) East (1976), no post-shock pressure gradient, incident flow Mach 1.4; (b) Seddon (1967), no post-shock pressure gradient, incident flow Mach 1.47; (c) present results, incident flow Mach 1.41.  Edge of supersonic tongue;  edge of boundary layer; δ_u , boundary-layer thickness before the interaction.

shock system different in shape and orientation to the flat-plate case. Both Seddon's and the present flow exhibit large supersonic tongues embedded in the subsonic flows downstream of the shock-wave systems; in these regions the flow is isentropically compressed to subsonic velocities. A large supersonic tongue was not expected in the present flow, because it had a lower Mach number (1.4) than Seddon (1.47), and previous results on flat-plate interactions at Mach 1.4 showed little to no supersonic flow behind the shock waves. East's (1976) data (figure 7a) did include a small post-shock supersonic region, but the Mach number here was ~ 1.01 . Data by Kooi (1975) for the same region in a very similar flow were Mach 0.02 lower. The appearance of a tongue in the present flow appears to be a result of the substantially different shock-wave pattern, which is a consequence of the post-shock pressure gradient. Kooi gathered his results with Pitot and static tubes, whereas East used a laser anemometer. It is interesting that the difference between these two sets of data ($\sim 2\%$) approximately equals the estimated uncertainty in the present Mach-number results (see table 1). As laser anemometry is the more accurate technique, the present measurements are probably slightly low in Mach number, which suggests that the size of the supersonic tongue may be larger than that shown in figure 7(c).

Figure 8 compares the displacement-thickness growth of the present flow in the interaction region with several flat-plate flows that have similar Mach and Reynolds numbers. As in figure 6, displacement-thickness data derived from profiles containing reversed flow have high uncertainty. However, even with a high uncertainty, it is clear that the post-shock adverse pressure gradient, by delaying the reattachment

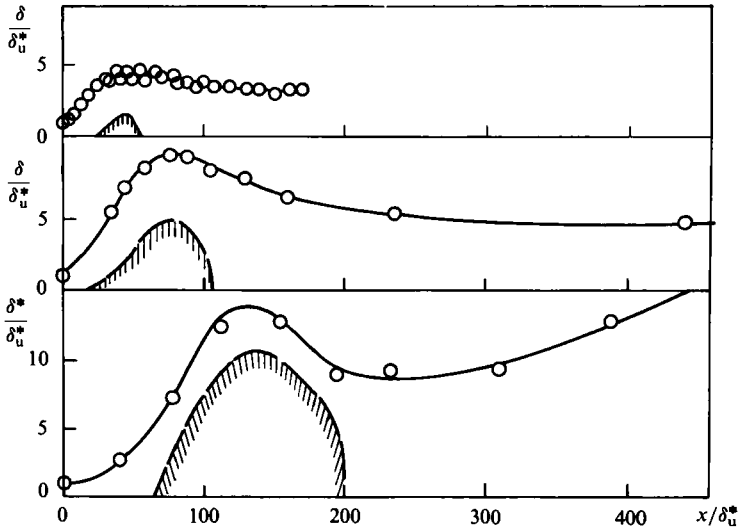


FIGURE 8. Displacement-thickness growth in the vicinity of the interaction: (a) Kooi (1975), Mach 1.40, Reynolds number at separation $Re_s = 20 \times 10^6$; (b) Seddon (1967), Mach 1.47, $Re_s = 3 \times 10^6$; (c) present results, Mach 1.41, $Re_s = 3.7 \times 10^6$; hatched , approximate edge of mean separated flow.

of the separated flow, causes a much larger separated region to form, and this has a major effect on boundary-layer growth through the interaction region. Downstream of reattachment (where data has better accuracy) the displacement thickness of a flat-plate flow continues to decrease as the layer relaxes back to zero-pressure-gradient conditions and the mean velocity near the wall increases. In the present flow, however, there are strong adverse pressure gradients acting downstream of reattachment, with high rates of mass entrainment into the layer, and, although the mean flow shows high rates of acceleration near the wall, there is a quite rapid increase in displacement thickness.

The skin-friction distribution[†] is also affected by a post-shock pressure gradient, but mainly in the recovery phase downstream of reattachment. Figure 9 compares skin-friction-coefficient results for an interaction on a flat plate (Seddon 1967) with the present results. Both flows separated extremely rapidly. In neither flow was the negative wall shear in the separation bubble measured. Vidal *et al.* (1973) did make measurements of reversed wall shear in a flat-plate flow using floating-element gauges. The quoted values for the reversed skin-friction coefficient are small ($\approx -0.5 \times 10^{-3}$) and have a high uncertainty. Downstream of reattachment, the distribution of skin friction is quite different between the two flows. Without a post-shock pressure gradient the wall stress overshoots its initial undisturbed value (figure 9a). Overshooting was also reported for the compression-corner case by Settles *et al.* (1976) and Muck & Smits (1983). In the present flow (figure 9b) the post-shock pressure gradient grossly retards the wall-shear recovery and, as shown later, it never recovers its undisturbed value.

Downstream of the interaction region, the main shock-interaction layer and the shock-free reference layer develop in identical adverse pressure gradients. However, these two downstream layers have quite different initial conditions, as only one has interacted with a shock wave. In order to compare the rate of boundary-layer growth of the two layers, the layer thicknesses at the end of the interaction region (taken

[†] Determined from Clauser charts with no allowance for compressibility.

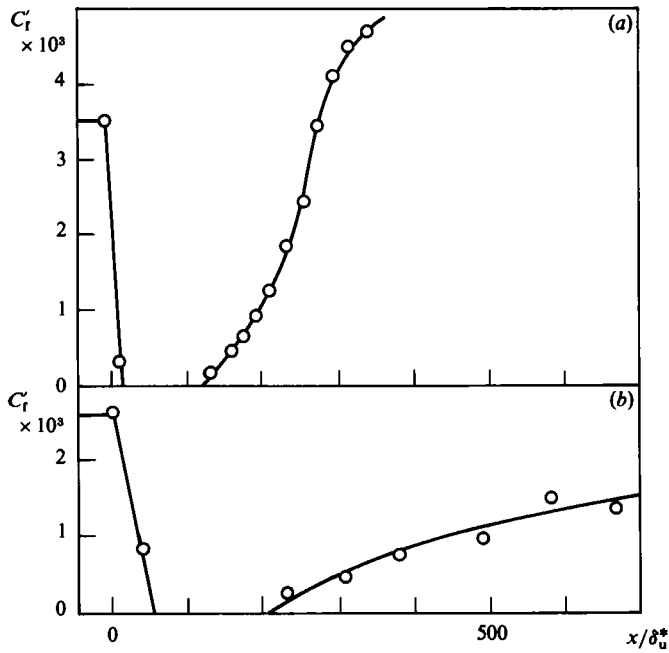


FIGURE 9. Skin-friction distributions in the vicinity of the interaction: (a) no post-shock pressure gradient (Seddon 1967); (b) strong post-shock adverse pressure gradient (present results).

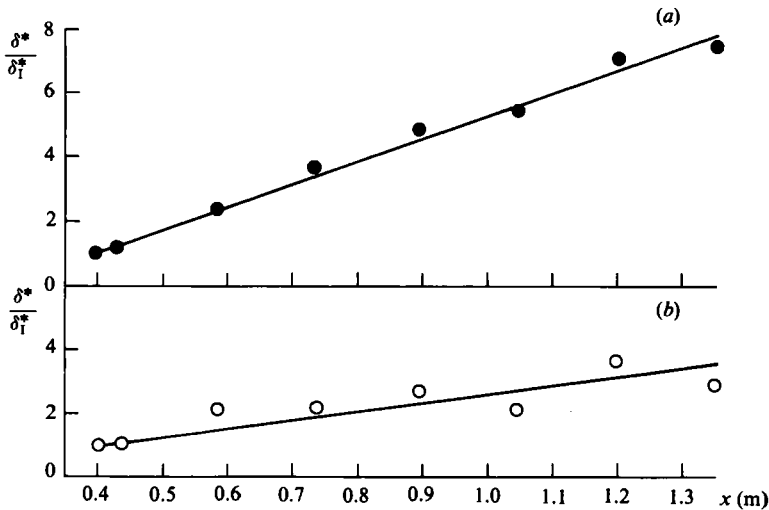


FIGURE 10. Displacement-thickness growth in the downstream region; δ_1^* = value of δ^* at $x = 0.4$ m: (a) shock-free reference layer ($\delta_1^* = 1.774$ mm); (b) shock-interaction layer ($\delta_1^* = 2.396$ mm).

as $x = 0.4$ m) were used to normalize the thicknesses. From the data shown in figure 10 it is obvious that in the downstream flow region the shock-free reference layer is growing much faster than the main interaction layer. This is a somewhat surprising result, as one may have expected a layer reattaching on a flat surface after separating and then having to negotiate a strong adverse pressure gradient would be held close to separation, with a corresponding high entrainment rate that would exceed that of a layer which had not been separated. In fact the opposite is the case. Another comparison of the downstream flow is shown in figure 11, where it can be

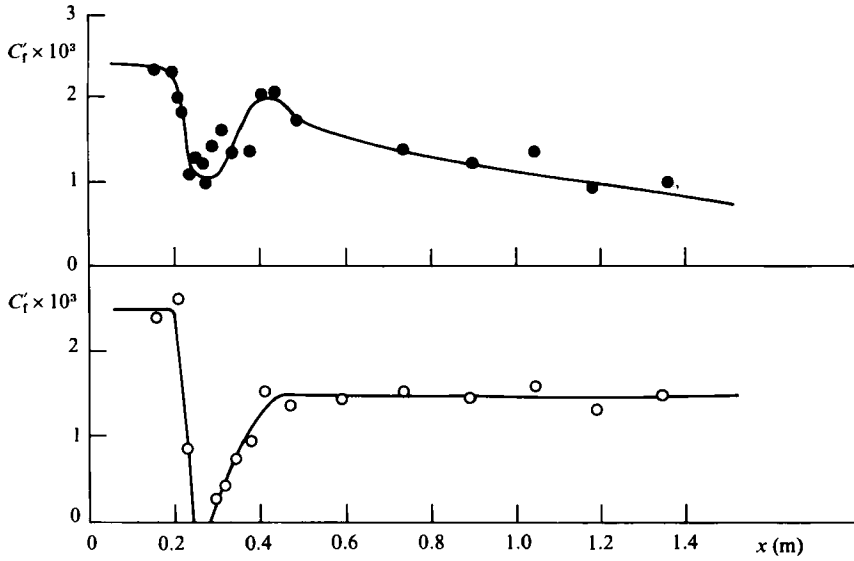


FIGURE 11. Skin-friction distributions in the downstream region:
(a) shock-free reference layer; (b) shock-interaction layer.

seen that the skin-friction distributions for the two layers are quite different. In this downstream flow region the shock-interaction layer is well attached, with a constant skin-friction coefficient, whereas the shock-free reference layer has a skin-friction coefficient that decreases with distance, and the layer appears to be approaching separation quite rapidly. Distributions of the standard mean profile shape parameters (form factor H , Clauser's G etc – see Schofield 1983) for the two layers also support the conclusion that the shock-free reference layer will separate well before the layer that has interacted with the shock wave. The most plausible explanation for these results is that the downstream development of the shock-interaction layer is modified by the two vortices that are shed into it from the interaction region. These vortices would lie within the layer and be most effective in stabilizing the downstream flow, increasing mixing within the layer and thereby reducing its entrainment. Similar vortices would be generated in a flat-plate interaction without a post-shock pressure gradient, and the enhanced mixing they generate would give rise to the overshoot of skin friction shown in figure 9(a).

We can obtain an estimate of the relative strength of the longitudinal vortices in the present experiment by evaluating the downstream entrainment rates in the layers with and without a shock interaction. The rate of volumetric increase in a boundary-layer flow is given by

$$\frac{dQ}{dx} = \frac{d}{dx} \int_0^{\delta} u \, dy = \frac{d}{dx} [U_1 (\delta - \delta^*)],$$

where dQ/dx is the volumetric entrainment rate of the layer per unit width and U_1 is the local free-stream velocity. If we again normalize with conditions at the start of the downstream region (δ_1^* and U_1 at $x = 0.4$ m) we can obtain

$$\frac{d}{dx} \frac{Q}{\delta_1^* U_1} = \frac{dQ_N}{dx} = \frac{U_1}{U_1} \frac{d}{dx} \frac{\delta - \delta^*}{\delta_1^*} - \frac{\delta - \delta^*}{\delta_1^*} \frac{d U_1}{dx} \frac{1}{U_1}.$$

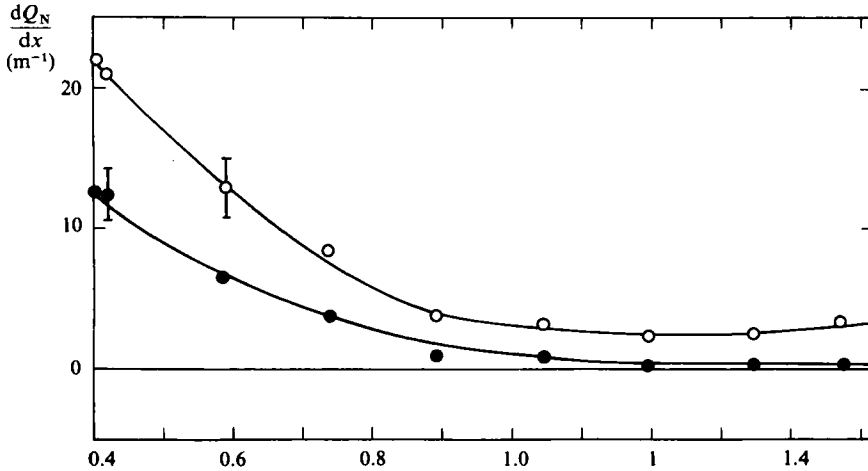


FIGURE 12. Entrainment-rate distributions: ●, shock-free reference layer; ○, shock-interaction layer; bar denotes range of uncertainty.

This normalized entrainment rate has been evaluated for the two flows, and is shown in figure 12. Although the uncertainty in the calculations is high (because they involve differentiation of experimental results), the trend is clear. The presence of the longitudinal vortices has drastically reduced the entrainment rate of the interaction layer, so that at large distances downstream of the interaction the entrainment is effectively zero. Here then, there is no irrotational fluid with free-stream velocity being brought into the layer, and the wall flow within the layer is reenergized by fluid with velocities less than the free stream. The fluid from the outer boundary layer is transported to the wall by two vortex systems acting at right-angles: the usual large-scale outer-flow coherent structures with axes transverse to the flow and the longitudinal vortices generated by the interaction with axes parallel to the flow. The two systems will of course interact, but the longitudinal vortices appear to be as strong as the usual large-scale vortex structure because together they hold skin-friction constant over a length in which it reduces by half in the reference flow without longitudinal vortices.

3.2. Temperature field

As the differences in total temperature between the flow and the wall were small and the probe was a simple shielded thermocouple, a check was made on the reliability of the instrumentation and techniques for measuring temperatures. This was done by measuring total-temperature profiles† in a shock-free supersonic favourable-pressure-gradient flow and comparing them with similar profiles by Meier & Rotta (1971), who made very careful measurements in such a flow using a sophisticated probe that drew air through a range of choked orifices. The present flow was generated by opening the rear flap of the duct to give an accelerating flow with Mach numbers up to Mach 2.3. This flow and the flow of Meier & Rotta both had mild favourable pressure gradients, were supersonic and nearly adiabatic. The present profiles (shown in figure 13) are very similar to the Meier & Rotta results, having a sinuous shape lying between lines for the simple linear Crocco relationship and the modified or parabolic Crocco relation and overshooting the free-stream stagnation temperature at high velocity ratios. The small sizes of the temperature overshoot imply a small heat loss from the experimental surface.

† And mean-velocity profiles.

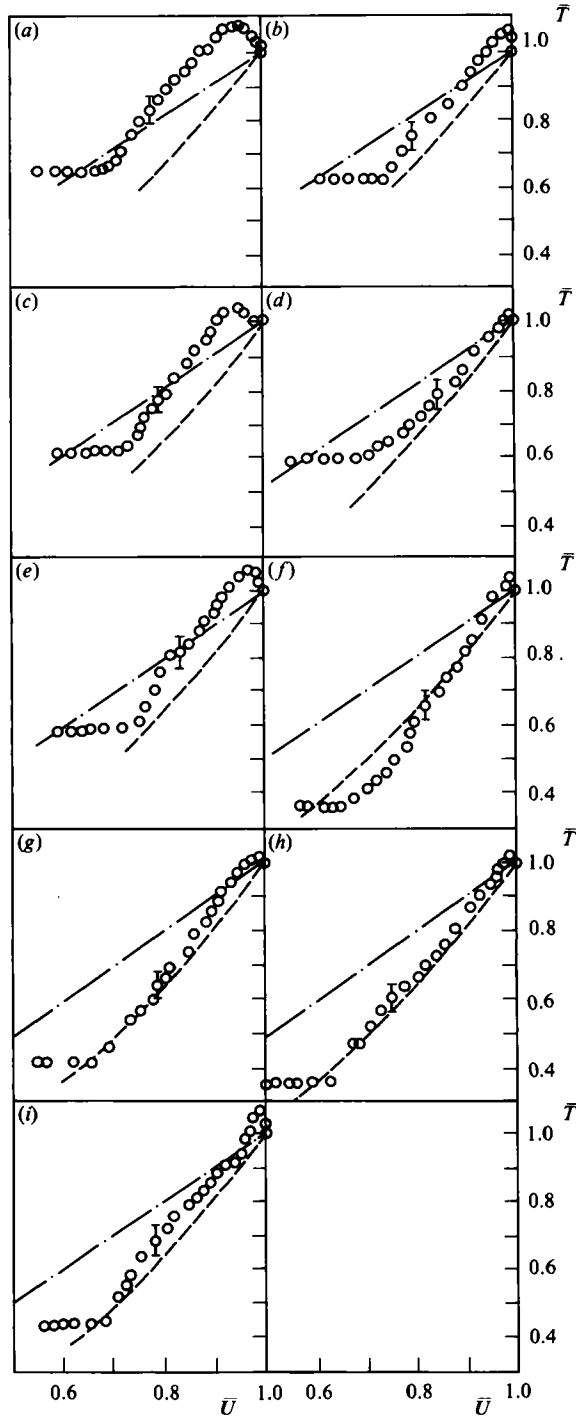


FIGURE 13. Boundary-layer temperature profiles for supersonic flow in a favourable pressure gradient: —, $T_p = T_0$; ---, $\bar{T} = \bar{U}$ (Crocco); - · - ·, $\bar{T} = \bar{U}^2$ (modified Crocco); $\bar{T} = (T_p - T_w)/(T_0 - T_w)$, where T_p is probe total temperature; T_w is the wall temperature, T_0 is the free-stream total temperature, $\bar{U} = u/U_1$ is the mean-velocity ratio. (a) $x = 0.225$ m; (b) 0.249 m; (c) 0.276 m; (d) 0.314 m; (e) 0.403 m; (f) 0.737 m; (g) 0.890 m; (h) 1.04 m; (i) 1.194 m. Bar denotes range of uncertainty.

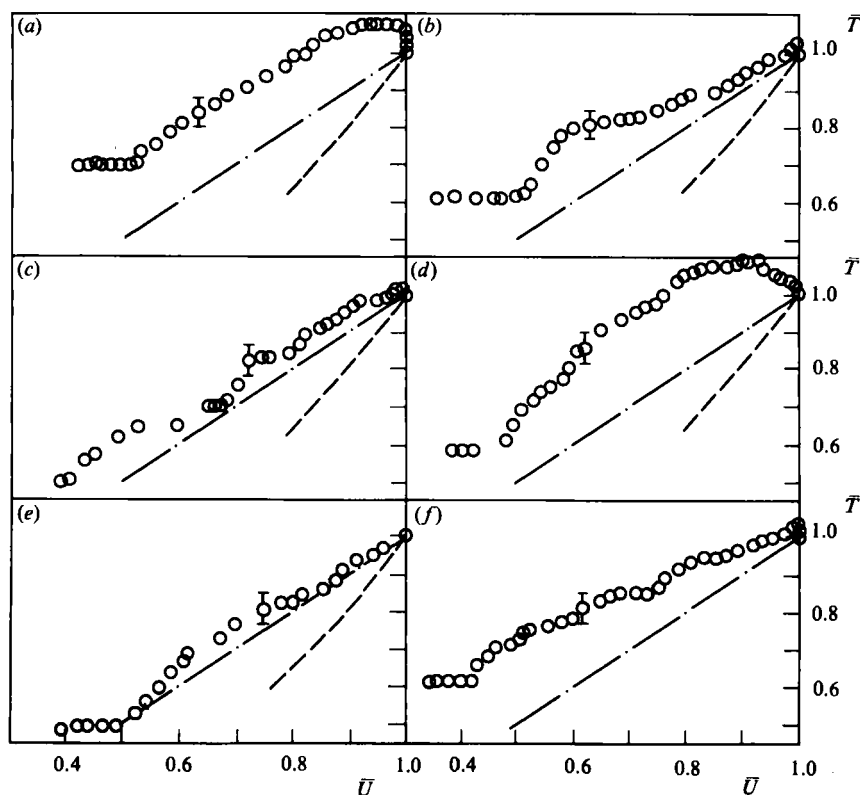


FIGURE 14. Boundary-layer temperature profiles for flow in a strong adverse pressure gradient. Symbols and notation as for figure 12. (a) $x = 0.403$ m; (b) 0.434 m; (c) 0.737 m; (d) 0.890 m; (e) 1.04 m; (f) 1.194 m. Bars denote range of uncertainty.

The profiles measured in the main adverse-pressure-gradient flow are different. Figure 14 shows profiles for the shock-interaction layer downstream of the separation bubble, and while these have a sinuous shape they all consistently lie above the linear Crocco line before overshooting the free-stream stagnation temperature. Profiles in the shock-free reference layer were similar (see Schofield 1983).

Profiles in the vicinity of the shock-wave interaction (figure 15) are unusual. The profile immediately before separation ($x = 0.225$ m) is a typical adverse-pressure-gradient profile, but the following profile ($x = 0.249$ m) passes through the separated-flow region and has an almost constant total temperature for the outer part of the profile above the recirculating flow. This result is consistent with the Reynolds-stress measurements of Simpson, Chew & Shivaprasad (1981), which showed that turbulent mixing rates were very high in a detached shear layer above a recirculating flow. The profile very close to reattachment ($x = 0.276$ m) has, by contrast, a large temperature overshoot and is adiabatic. The flow at this point is similar to a stagnation-point flow on an adiabatic wall. The final profile in figure 15 ($x = 0.314$ m) was taken downstream of reattachment, where the flow was undergoing rapid acceleration near the wall, and this has reduced the total temperatures across the profile.

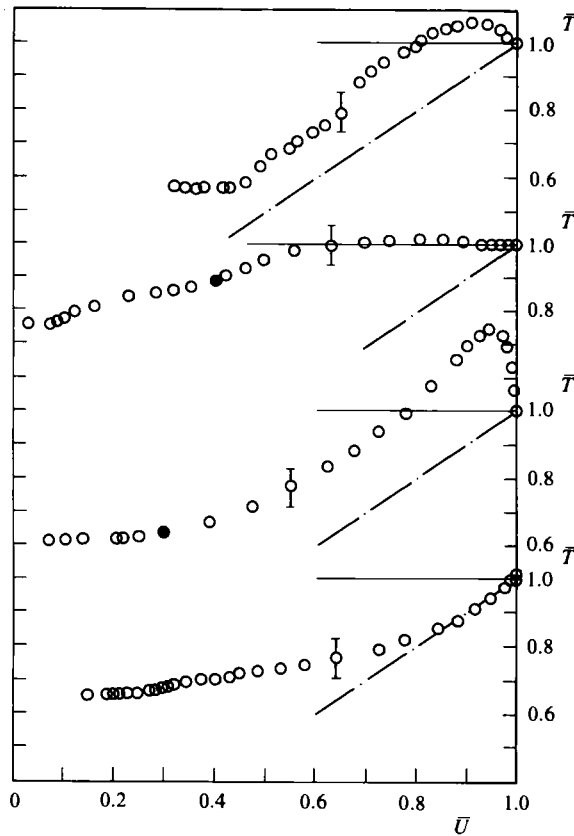


FIGURE 15. Boundary-layer temperature profiles for flow in the vicinity of a shock-wave-boundary-layer interaction. Symbols and notation as for figure 12. (a) $x = 0.225$ m; (b) 0.249 m; (c) 0.276 m; (d) 0.314 m. Bars denote range of uncertainty.

4. Conclusion

An obvious conclusion of this work is that the separate effects of a normal shock wave and an adverse pressure gradient in a rectangular duct cannot be used in any simple way to predict their combined effect on the development of the turbulent layers. Specifically, the two agencies in a duct flow do not combine to produce a boundary layer that is more likely to reattach downstream of the shock wave, but instead the interaction acts as a strong stabilizing agency for the downstream boundary layer. The flow investigated here had strong three-dimensional components, and it could therefore be considered that this conclusion was specific to laterally constrained flows and would not apply to, for instance, axisymmetric flows in air intakes or supersonic diffusers. However, if such an axisymmetric flow involves a sizeable separated region then it is likely that Taylor-Görtler vortices will be generated over the rear of the separation bubble as a consequence of the change in angular velocity in this region. This vorticity will be augmented by the increased mixing that occurs across any shock wave interacting with a turbulent boundary layer (even in the non-separating axisymmetric case – see Hayakawa, Smits & Bogdonoff 1982; Rose & Childs 1974). In addition, any separated flow becomes strongly three-dimensional downstream of detachment (Kline, Bardina & Strawn 1983), even where great trouble has been taken to preserve the two-dimensionality of a flow (see Simpson *et al.* 1981). Large turbulent structures, mixing fluid across the flow,

appear to be a feature of separated layers (Simpson *et al.* 1981). For interaction flows that are only nominally two-dimensional, such as high-aspect transonic wings, it seems likely that three-dimensional cellular flows could be formed. In such flows the inherent tendency of separated layers to become three-dimensional would be enhanced and probably ordered into cells by the continuous variation in geometry along the wing. If this is the case, we could expect pairs of counter-rotating vortices emanating from cells (similar to the one in figure 2) spaced along the wing. In a transonic compressor, where the effective Mach number as well as the flow geometry varies rapidly with increasing radius, the tendency for the interaction region to divide laterally into three-dimensional cells would be considerably stronger. The level of shed vorticity would in this case vary with radius. It therefore seems likely that any shock-wave-boundary-layer interaction that involves separation irrespective of its geometry will shed sufficient vorticity into the downstream flow to increase its stability substantially. These speculations are supported by the work of Livesey & Odukwe (1974), Kamal, Odukwe & Livesey (1974) and Kamal & Livesey (1977), who measured the performance of a range of subsonic axisymmetric diffusers preceded by a long pipe. They found that if the inlet pipe contained shock waves then the diffusers gave higher pressure recoveries with lower flow distortion, i.e. the boundary layers entering the diffusers were thinner and better attached. They attributed this stabilization to the (measured) increased turbulence levels in the flow with shock waves.

Another aspect of the interaction between shock wave and downstream pressure gradient is the major modification to the structure of the interaction region caused by the downstream pressure gradient. By delaying the reattachment of the shock-induced separation, the downstream pressure gradient causes an interaction region to be generated that is significantly different from corresponding regions in flows at similar Mach and Reynolds number, but without post-shock pressure gradients. Thus calculations of boundary-layer development based on results of an interaction without a post-shock pressure gradient coupled with a separate calculation of boundary-layer growth in the adverse pressure gradient are likely to be in gross error.

The present results are probably not relevant to the case where the normal shock wave is too weak to cause a separated region to form in the boundary layer. Here the adverse effects of shock wave and post-shock pressure gradient on boundary-layer development may well be cumulative. Paradoxically, it may be better for high component performance to have a strong normal shock wave producing a local separation, as this has the same effect as the installation of vortex generators at the start of the subsonic pressure rise.

Finally the temperature profiles give an appreciation of how the temperature-velocity relationship in a compressible layer is affected by the sign of the pressure gradient. It is unusual to be able to compare profiles such as these that were taken in the same flow geometry with the same instrumentation, differing only in the sign of the pressure gradient applied to the flow. They suggest that favourable-pressure-gradient profiles have a sinuous shape and lie between the linear and parabolic Crocco relations. As the favourable pressure gradient becomes stronger (nearer the exit of the duct) the profiles approximated to the parabolic distribution. In an adverse pressure gradient the profiles were well removed from the parabolic distribution and lay between the linear Crocco and constant-total-temperature lines. However, within the interaction region the profiles appeared to respond strongly to local flow conditions, being quite different from the previous results, but also differing markedly between themselves.

REFERENCES

- ALSTATT, M. C. 1977 *AEDC Rep.* AEDC-TR-77-47.
- BROWN, A. C., NAWROCKI, H. F. & PALEY, P. N. 1968 *J. Aircraft* **5**, 221.
- CHEN, C. P., SAJBEN, M. & KRONTIL, J. C. 1979 *AIAA J.* **17**, 1976.
- EAST, L. F. 1976 *RAE TM* 1666.
- GREEN, J. E. 1969 *RAE TR* 69098, p. 7.
- HAYAKAWA, K., SMITS, A. J. & BOGDONOFF, S. M. 1983 In *Structure of Complex Turbulent Shear Flow* (ed. R. Dumas & L. Fulachier), p. 279. Springer.
- HAYAKAWA, K. & SQUIRE, L. C. 1982 *J. Fluid Mech.* **122**, 369.
- HUNT, J. C. R., ABELL, C. J., PETERKA, J. A. & WOO, H. 1977 *J. Fluid Mech.* **86**, 179.
- INGER, G. R. 1975 *Final Rep. to Office of Naval Research; Contract* NOO14-75-C-0456.
- KAMAL, W. A. & LIVESSEY, J. L. 1977 In *Proc. Symp. on Turbulent Shear Flows, University Park, Pennsylvania State Univ. Pennsylvania*, p. 12.1.
- KAMAL, W. A., ODUKWE, A. O. & LIVESSEY, J. L. 1974 In *Proc. 5th Australasian Conf. on Hydraulics and Fluid Mechanics, Christchurch*, p. 98.
- KLINE, S. J., BARDINA, J. G. & STRAWN, R. C. 1983 *AIAA J.* **21**, 68.
- KLINE, S. J., CANTWELL, B. J. & LILLEY, G. M. (eds.) 1982a *Proc. AFOSR-HTMM-Stanford Conf. on Complex Flows*, vol. i. Stanford University.
- KLINE, S. J., CANTWELL, B. J. & LILLEY, G. M. (eds.) 1982b *Proc. AFOSR-HTMM-Stanford Conf. on Complex Flows*, vol. ii. Stanford University.
- KLINE, S. J., CANTWELL, B. J. & LILLEY, G. M. (eds.) 1982c *Proc. AFOSR-HTMM-Stanford Conf. on Complex Flows*, vol. iii. Stanford University.
- KLINE, S. J. & McCLINTOCK, F. A. 1953 *Mech. Engng* **75**, 3.
- KOOI, J. W. 1975 In *Proc. AGARD Symp. on Flow Separation; AGARD CPP-168*. Also NLR-MP-78013U (1978).
- LEBLANC, R. & GEOTHALS, R. 1975 *NASA TTF* 16698.
- LIVESSEY, J. L. & ODUKWE, A. O. 1974 *Proc. Inst. Mech. Engrs* **188**, 607.
- MEIER, H. U. & ROTTA, J. C. 1971 *AIAA J.* **9**, 2149.
- MUCK, K. C. & SMITS, A. J. 1983 In *Proc. 4th Symp. on Turbulent Shear Flows, Karlsruhe*. Springer-Verlag.
- PADOVA, C., FALK, T. J. & WITTLIFF, C. E. 1980 *AIAA Paper* 80-0158.
- PERRY, A. E. & FAIRLIE, B. D. 1974 *Adv. Geophys.* **B18**, p. 299. Academic.
- ROSE, W. C. & CHILDS, M. E. 1974 *J. Fluid Mech.* **65**, 177.
- SAJBEN, M. & KRONTIL, J. C. 1981 *AIAA J.* **19**, 1386.
- SCHOFIELD, W. H. 1975 *ARL Mech. Engng Note* 359.
- SCHOFIELD, W. H. 1983 *ARL Mech. Engng Rep.* 161.
- SEDDON, J. 1967 *ARC R & M* 3502.
- SETTLES, G. S., VAS, I. E. & BOGDONOFF, S. M. 1976 *AIAA J.* **14**, 1709.
- SETTLES, G. S., WILLIAMS, D. R., BACA, B. K. & BOGDONOFF, S. M. 1982 *AIAA J.* **20**, 60.
- SIMPSON, R. L., CHEW, Y. T. & SHIVAPRASAD, B. G. 1981 *J. Fluid Mech.* **113**, 23.
- VIDAL, R. J. & KOOI, J. W. 1976 *NLR Rep.* AC-76-02.
- VIDAL, R. J., WITTLIFF, C. E., CATLIN, P. A. & SHEEN, B. H. 1973 *AIAA Paper*-73-661.